ResearchGate

See discussions, stats, and author profiles for this publication at: https://www.researchgate.net/publication/263952404

Facile Synthesis of Smart Magnetic Graphene for Safe Drinking Water: Heavy Metal Removal and Disinfection Control

ARTICLE *in* ACS SUSTAINABLE CHEMISTRY & ENGINEERING · MARCH 2013

Impact Factor: 4.64 · DOI: 10.1021/sc300112z

CITATIONS
44

READS
305

3 AUTHORS, INCLUDING:

Ganesh Gollavelli
Andhra University
4 PUBLICATIONS **154** CITATIONS

SEE PROFILE

Available from: Ganesh Gollavelli
Retrieved on: 03 February 2016

ACS Sustainable Chemistry & Engineering

Research Article

pubs.acs.org/journal/ascecg

Facile Synthesis of Smart Magnetic Graphene for Safe Drinking Water: Heavy Metal Removal and Disinfection Control

Ganesh Gollavelli,[†] Chun-Chao Chang,[‡,§] and Yong-Chien Ling*[,†]

[†]Department of Chemistry, National Tsing Hua University, Hsinchu 30013, Taiwan

[‡]Department of Internal Medicine, School of Medicine, College of Medicine, Taipei Medical University, Taipei 11031, Taiwan

[§]Division of Gastroenterology and Hepatology, Department of Internal Medicine, Taipei Medical University Hospital, Taipei 11031, Taiwan

Supporting Information

ABSTRACT: Bacterial infections, the toxicity of engineered nanomaterials, the presence of inorganic pollutants in the environment, and providing safe drinking water are the most threatening problems of the 21st century. To tackle these challenges, we develop a one-pot, solvent free, and rapid synthesis of smart magnetic graphene (SMG) by microwave irradiation of graphene oxide (GO) and ferrocene precursors. The SMG possesses increased adsorption sites with tunable superparamagnetic properties (50 emu/g, 1:7 wt %), facilitating the adsorption and magnetic separation of aqueous Cr(VI), As(V), and Pb(II) with ~99% removal efficiencies down to the 1 ppb level. The X-ray photoelectron spectroscopy (XPS) analysis of SMG-Cr(VI) reveals the reduction of Cr(VI) to Cr(III), presumably due to the surface phenolic groups and unprotected ferrous ions on the SMG surface. The maximum adsorption capacity of SMG is 4.86, 3.26, and 6.00 mg/g for respectively Cr(VI), As(V), and Pb(II) at an initial concentration of 5.0 ppm. The addition of KNO_3 does not affect Cr(VI) adsorption efficiency; whereas Na_2SO_4 shows a decreasing trend on Cr(VI) adsorption. The SMG exhibits disinfection action (40 μg/L) toward *E. coli* bacteria with 100% killing efficacy and low toxicity (0.1 ng/nL) toward zebrafish without inducing any abnormalities. The SMG is reusable and successfully works on drinking water sources, suggesting that SMG is a preferred adsorbent for safe drinking water.

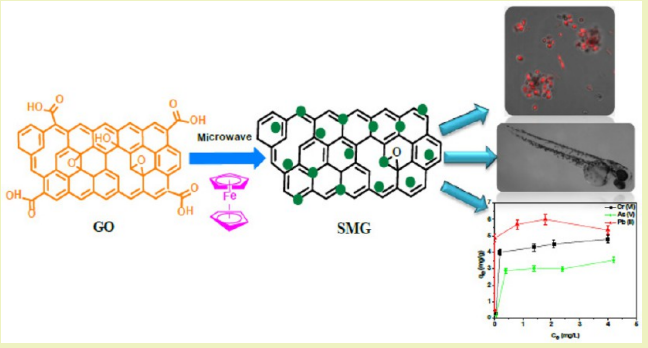

KEYWORDS: *Magnetic graphene, Green chemistry, Heavy metal removal, Biocompatible, Disinfection, Safe drinking water*

INTRODUCTION

A incessant supply of potable and safe drinking water is on the top notch[1] among many globally pervasive and emerging risks such as microbial infections,[2] environmental impact of engineered nanomaterials (NMs),[3] and inorganic/organic contaminants.[4] The contaminants usually enter downstream waters through rapid industrialization and natural microbes, ultimately leading to the deterioration of public human health.[5] Many efforts have been driven to decontaminate the potable water. The need for an efficient, cost-effective, robust, and handy technology for the decontamination of downstream water without endangering human health is still tremendous.[6] The centralized water system (CWS) generally involves purification procedures such as chlorination, ozonolysis, UV irradiation, and electrochemical methods which often need huge investment for infrastructures and energy for operation. Moreover, the formation of hazardous disinfection byproducts such as chlorine and chloramines during chlorine disinfection is of high concern.[7] Many obstacles are therefore anticipated when promoting a decentralized water system by adopting current CWS purification technology.[8] To address these complications, the development of smart adsorbents with excellent removal capability toward toxic contaminants such as heavy metals and persistent organic pollutants,[9] disinfection activity to prevent microbial infections, and biocompatibility to humans through the supply of potable and safe drinking water is warranted. Recently, removal of heavy metals such as chromium, arsenic, and lead have been especially challenging owing to their high toxicity and potential carcinogenicity. The current regulatory limits of the U.S EPA for these heavy metals in drinking water are 100 ppb for Cr(VI), 10 ppb for As(V), and 15 ppb for Pb(II); whereas WHO lowers the limits to 50 ppb for Cr(VI) and 10 ppb for Pb(II).[10−12] There are numerous purification methods such as adsorption, bioremediation, precipitation, reverse osmosis, and ion-exchange being developed for heavy metal removal. Among them, the adsorption method is relatively simple and cost-effective.[13,14] Conventionally, activated carbon is a widely used adsorbent to

Received: October 11, 2012
Revised: February 6, 2013
Published: March 5, 2013

ACS Publications © 2013 American Chemical Society

treat contaminated waters; however, it is inefficient to remove the contaminants down to the parts per billion (ppb) level.[15] Adopting lucrative purification methods for the removal of heavy metals down to the ppb level has become primarily important. Nanoscale iron and iron oxide structures have proven to be better adsorbents for heavy metals with high efficiencies.[16,17] The drawbacks such as being prone to air oxidation and difficulties in recyclability restrict their practical applications.[18] Several NMs with dye or metal adsorption properties,[19,20] antibacterial/fungal activity,[21] and toxicity/biocompatibility issues[22] have been reported. Moreover, the critical issues of environmental impact and human health risk during their life cycle have seldom been discussed.

Graphene has attracted tremendous research interest due to its large surface area, high carrier transport mobility, superior mechanical flexibility, and excellent conductivity in both heat and electricity.[23] These intriguing properties of graphene have expanded its applications from electronics to the biology and environmental fields.[24,25] Existing methods reported for the exfoliation of graphene sheets involved peeling,[26] chemical,[27] and thermal reduction methods.[28] The sonochemical and microwave-assisted processes provide a feasible and greener alternative to complement conventional approaches.[29,30] The introduction of magnetic properties into NMs and their composites accelerating their applications in environmental monitoring[31,32] and treatment technologies[33] were well-established. A magnetic graphene/graphene oxide (GO) nanocomposite has recently been explored for the removal of heavy metal and organic dyes. For example, GO/Fe composites prepared with different Fe loading have been utilized for efficient removal of arsenate ions.[34] Water-dispersible magnetite-reduced GO composites and graphene-based multifunctional iron oxide nanosheets have been successfully demonstrated for As(III), As(V), and Cr(VI) removal.[19,35] Nanoscale zerovalent iron decorated on graphene sheets has been used for enhanced Cr(VI) removal.[36] A one-pot synthesis method was adopted to synthesize graphene decorated with core@double shell nanoparticles for fast Cr(VI) removal.[37] Magnetite/GO composites for efficient Co(II), Cu(II), and fulvic acid removal has been successfully demonstrated.[38,39] Graphene from sugar and reduced graphene oxide-metal/metal oxides were also demonstrated for water purification.[40,41] The aforementioned composites have been successfully utilized for heavy metal or organic pollutants removal. Factors relevant to safe drinking water including antifouling activity, in vivo toxicity, and removal efficiencies down to the ppb level were seldom being considered. Moreover synthetic strategies to overcome long reaction times, high temperatures, and noxious reducing agents[19,34−37,42] are also warranted. These requirements inspired us to design a green one-pot synthesis promoting the reduction and magnetization of GO in a single step to yield smart magnetic graphene (SMG), exhibiting advantageous properties for simultaneous heavy metal removal, disinfection control, and biocompatibility for safe drinking water. To the best of our knowledge, there is no report producing magnetic graphene within a minute by a green approach with effective antibacterial activity and in vivo compatibility with multimetal removal capability down to the ppb level.

Herein, we introduce rapid and green synthesis of SMG, which allows simultaneous reduction and magnetization of GO within one minute. The graphitized iron nanoparticles (NPs) were homogenously sandwiched onto the graphene surface yielding increased adsorption sites with tunable superparamagnetic property. The capability of SMG as a heavy metal adsorbent, disinfectant, biocompatibility, recyclability, and use for drinking water source samples were subsequently tested and demonstrated. Overall, the discovery of SMG would provide new solutions to the safe drinking water problems of the 21st century.

EXPERIMENTAL SECTION

Materials. Graphite flakes (99%) and ferrocene (99%) were purchased from Alpha Aesar. Sodium nitrate (98.5%) from Showa chemicals, potassium permanganate (99%) from BDH Ltd., potassium dichromate ($K_2Cr_2O_7$, 99.99%), sodium arsenate (Na_2HAsO_4), $PbCl_2$ from High Purity Standards, hydrogen peroxide (30%) from Sigma Aldrich, and H_2SO_4 (98%) from Fluka were purchased. DAPI (4′,6-diamidino-2-phenylindole) and PI (propidium iodide) were purchased from Invitrogen.

Preparation of SMG by the Solid-State Microwave Induced Process. GO was prepared following the Hummers process by using pristine graphite flakes as a starting material.[43] The SMG was obtained by adding GO (50 mg) and ferrocene (150 mg) to a quartz tube containing broken silicon wafers (20 pieces), evacuated under vacuum for 30 min, irradiated inside a focus microwave oven (2.45 GHz, Discover system, CEM corporation) under a nitrogen atmosphere (1 atm) for 1 min with 20 s intervals each. During irradiation, violent arcing occurred between the silicon wafers, leading to the decomposition of ferrocene and reduction of GO to yield SMG. The residual ferrocene was removed from free carbon soot with toluene/acetone, and the product was collected by an external magnet. This process was repeated twice to remove the residual ferrocene completely. Later, the contents were washed with conc. HCl to etch away the free iron from the products, and finally washed with one toluene/acetone to stop the etching. The purified SMG was dried under vacuum and subjected to various characterizations.

Characterization. For electron microscopy measurements, high-resolution transmission electron microscopy (HRTEM, 200 keV, JEOL, JEM-2100) and scanning electron microscopy (SEM, JEOL, JSM-7000F, FESEM) were used. The saturation magnetization of SMG was measured with a superconducting quantum interference device (SQUID, Quantum Design, model MPMS5). The powder X-ray diffraction patterns were recorded with an XRD operated with Cu Kα radiation (Shimadzu XRD-6000). Raman studies were done with a Micro Raman (Renishaw) equipped with a 630 nm laser. High-resolution X-ray photoelectron spectroscopy (HRXPS) measurements were measured with a PHI Quantera SXM, scanning X-ray microprobe (ULVac-PHI Inc.). Brunauer−Emmett−Teller (BET) surface area measurements were carried out using a BELCAT-B (BEL JAPAN. INC). Fourier transform infrared (FT-IR) spectra were recorded using a FT-IR spectrometer (Bomem model, DA-83FT). Thermal gravimetric analysis was measured using a TGA/MS (Linseis Pt-1600). Trace amounts of heavy metals were detected using an inductively coupled plasma-mass spectrometer (ICP-MS, Thermo Scientific, X-Series II). Incubation of bacterial culture was carried out using an orbital shaking incubator (KS, 0S1500X).

Adsorption of Cr(VI), As(V), and Pb(II) by SMG. Stock solutions (1000 ppm) of Cr(VI), As(V), and Pb(II) heavy metals were prepared in doubly distilled water. Batch removal studies were carried out at the desired adsorption time and adsorbent dosage levels at the initial concentrations ranging from 0.1−5.0 ppm. An aliquot of SMG (5 mg) was directly added into heavy metal solution (25 mL), sonicated for ∼3 min at room temperature, and finally subjected to orbital shaking for ∼2 h at 300 rpm. At the end of adsorption, the suspension was separated by using an external magnet. The heavy metal concentrations prior to and after adsorption were determined by ICP-MS. Experimental conditions such as initial concentration, pH, and adsorption time were optimized to evaluate the adsorption efficacy. All adsorption experiments were carried out in four replicates. The repeatability was expressed as relative percentage deviation. The amount of heavy metals adsorbed per unit mass of the adsorbent was evaluated by using the following equation: $q_e = (C_o - C_f)V/M$ where

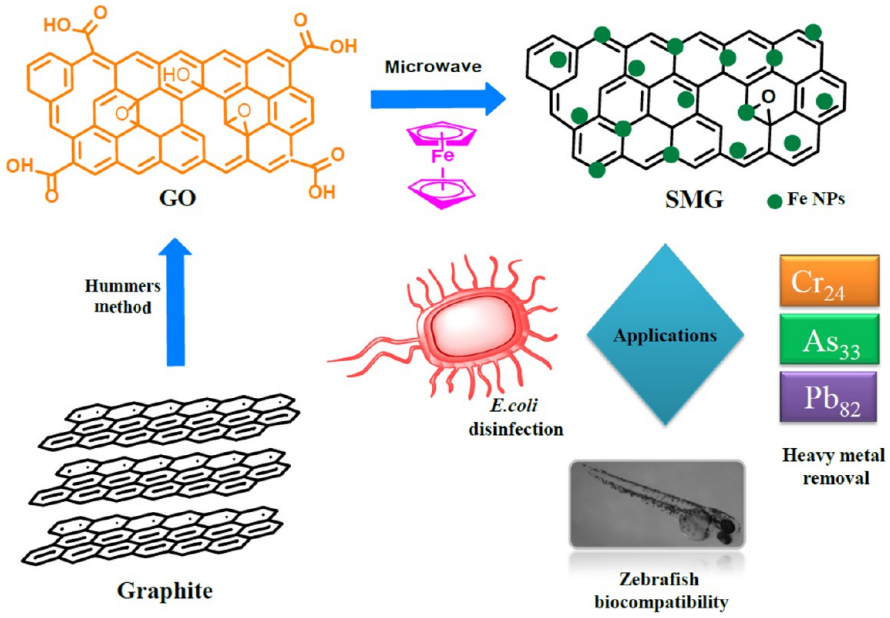

Figure 1. Schematic for the synthesis of SMG from GO obtained by Hummers method followed by one-pot microwave-assisted reduction and magnetization and safe drinking water applications.

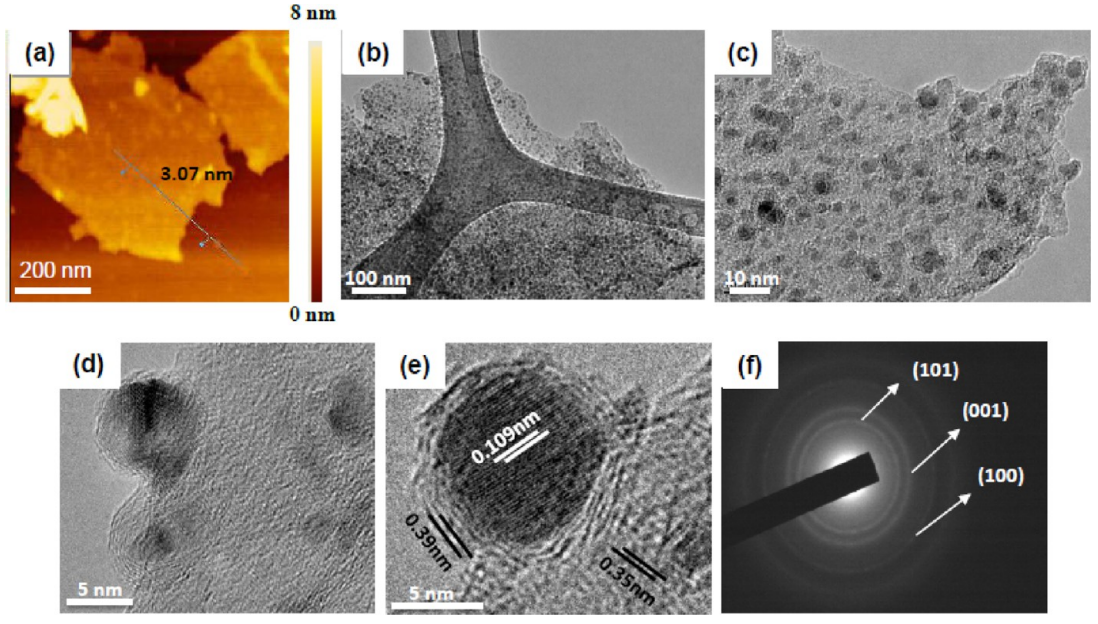

Figure 2. AFM and TEM analyses of GO and SMG: (a) AFM image of GO, (b) low- and (c) high-magnification TEM images of SMG, (d) TEM image of SMG showing Fe NPs embedded in graphene sheet, (e) HR-TEM image showing close view of lattice fringes around the Fe NPs, and (f) SAED ring pattern of graphene sheet embedding Fe NPs.

q_e (mg/g) is the amount of heavy metals adsorbed per gram of adsorbent, C_o and C_f represent the initial and final heavy metal concentration after adsorption, V is the solution volume (mL), and M is the adsorbent weight (g). The drinking water source (DWS) samples were prepared by premixing different amounts of respective Cr(VI) (150 ppb), As(V) (50 ppb), and Pb(II) (50 ppb) solutions and subsequently diluted to permissible DWS concentration. An aliquot of DWS (25 mL) was treated with SMG (5 mg). The effect of salt was studied by adding an appropriate amount of Na_2SO_4 and KNO_3. The recycling experiments were carried out by washing the used adsorbent with KOH (0.01 M) and HCl (0.01 M) solutions to remove the adsorbed metals.

Disinfection Control. *E.coli* (*Escherichia coli*) bacterial cells (OD_{600} ~ 0.2) were diluted 10^4 times in NaCl solution (0.9%, corresponding to ~10^8 cfu/mL) and added to different concentrations of SMG in 1.5 mL tubes. Aliquots (100 μL) were plated onto agar plates for 0, 1, and 2 h, respectively. The prepared bacterial plates were incubated in the orbital shaking incubator at 37 °C for 15−18 h. After incubation, the number of bacterial colonies (cfu/mL) were counted visually and converted to corresponding cell viabilities.

Confocal Microscopy. Aliquots of NaCl solution (1 mL 0.9%) containing bacterial cells (~10^8−10^9) were taken and centrifuged at 8000 rpm for 5 min. The supernatant was discarded, and the pellet was resuspended in aqueous *p*-HCHO (para-formaldehyde) solution (2%, 300 μL) in NaCl solution (0.9%) and kept standing for 30 min at room temperature. The samples were centrifuged again for 5 min, added with DAPI solution (20 mg/mL, 50 μL) and PI (0.5 mg/mL, 20 μL), and incubated in the dark for ~15 min. The contents were

dx.doi.org/10.1021/sc300112z | ACS Sustainable Chem. Eng. 2013, 1, 462−472

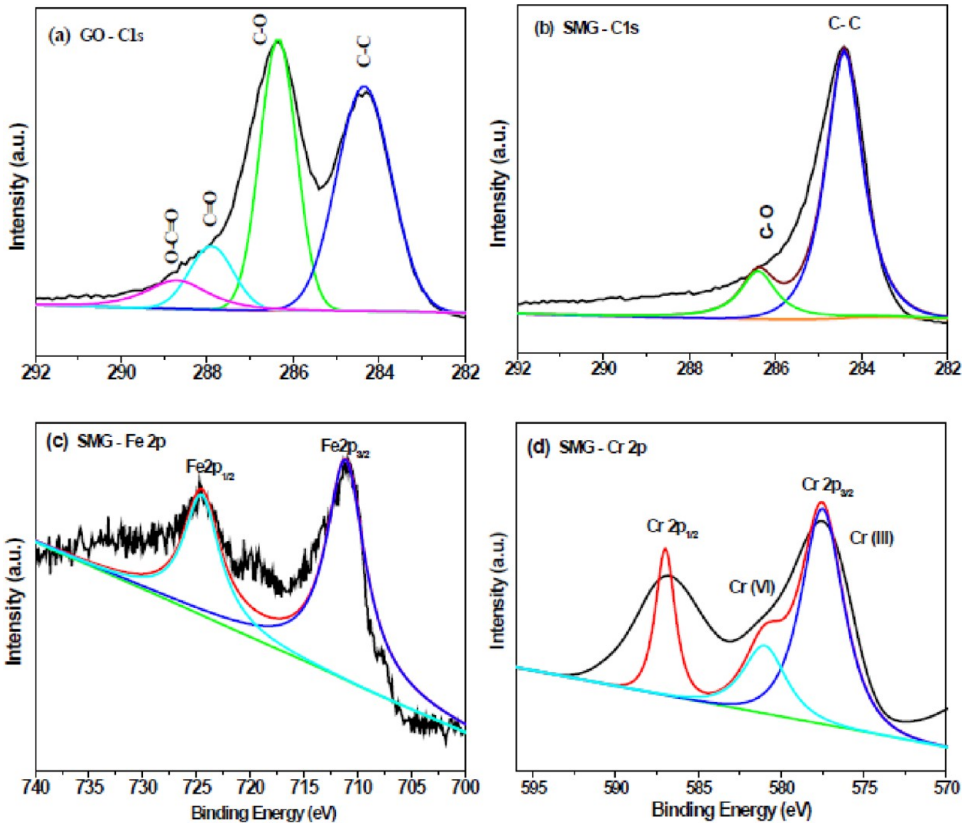

Figure 3. HRXPS spectra (a) C1s of GO, (b) C1s of SMG, (c) Fe2p of SMG, and (d) Cr2p of SMG-Cr.

centrifuged, and the supernatant was discarded. The pellet was resuspended in a small amount of water. The stained bacterial solution was collected with a micropipet. A small drop was placed on the glass slide with the coverslip on it. The samples were visualized using a confocal scanning laser microscope (CLSM, Zeiss, LSM 700) equipped with an InGaN semiconductor laser (405 nm), an Ar laser (488 nm), and a He−Ne laser (543 nm) to identify the live and dead bacterial cells operated with a 100× objective lens.

Zebrafish Biocompatibility. *Danio rerio* (zebrafish) embryos (Wild-type AB strains) obtained from zebrafish core facility center at National Tsing Hua University were used in all experiments. The fresh embryos were collected onto the microinjection embryo tray just before the experiment. The SMG stock solutions were prepared in doubly distilled water and sonicated until microinjection. About 10 nL volume was microinjected into the zebrafish pole region of embryos between stage 1 (one cell embryo) and 3 (four cell embryo) using a Drummond microinjector. A total of 50 embryos were used for each experimental condition. The microinjected embryos were transferred onto the petri dish filled with system water and incubated at 28 °C in the dark. For the in vivo toxicity tests, live embryos were counted each day until 120 hpf (hours postfertilization). After 120 hpf, all developed embryos were examined by fluorescence microscope (Nikon, E600) to visualize any phenotypic changes.

RESULTS AND DISCUSSION

Preparation and Characterization of SMG. A schematic (Figure 1) illustrates the one-pot and solvent-free synthesis of SMG by microwave-assisted solid-state reaction. The GO and ferrocene powders served as precursors using small pieces of silicon (Si) wafers as susceptors to initiate the microwave irradiation. Upon irradiation, GO tended to be reduced and became graphene by eliminating the surface oxygen functional groups. In the meantime, the decomposition of ferrocene was initiated and led to the formation of a metallic Fe core (~5 nm in size).

The microwave operated in pulsed mode creates an atmosphere of simultaneous rapid heating and cooling, preventing the agglomeration of Fe NPs, further promoting the low dense carbon atoms to graphitize the Fe core.[44] The synthesis of SMG follows a template-growth model, in which, the Fe core is formed first and serves as a template for latter graphitization.[45] The simultaneous reduction and magnetization of GO was carried out within 1 min. The advantages of the present strategy were compared with the reported methods (Supporting Information Table S1). Figure 2a shows the AFM image of GO with ~3 nm thickness corresponding to 1−3 layers. The morphology of SMG was examined using TEM. Figure 2b and c represents the respective low- and high-magnification TEM images of SMG, showing graphene layers being wrinkled and decorated with uniformly dispersed Fe NPs with a mean particle size of ~4.5 nm (Supporting Information Figure S1). Figure 2d represents the HR-TEM image of SMG, showing graphene layers coiled at the interface of graphene sheet and Fe NPs embedded inside rather than simply adhering physically or blending into the graphene sheet. This could further prevent the embedded Fe NPs from atmospheric air oxidation and acid corrosion. The apparent lattice fringes in the HR-TEM image (Figure 2e) reveals the graphene shell (0.39 nm *d*-spacing) of Fe NPs sandwiched into the graphene sheet (0.35 nm *d*-spacing); whereas the 0.109 nm *d*-spacing could be indexed to Fe NPs. The selected area electron diffraction (SAED) ring pattern (Figure 2f) confirms its structure as polycrystalline Fe with orthorhombic structure based on (101), (001), and (100) crystal planes along the zone axis [001].

dx.doi.org/10.1021/sc300112z | *ACS Sustainable Chem. Eng.* 2013, 1, 462−472

HR-XPS was used to investigate the surface chemical composition of GO, SMG, and Cr(VI)-adsorbed SMG (SMG-Cr) (Supporting Information Figure S2a). The HR-XPS C1s spectrum of GO (Figure 3a) shows peaks at 286.3 eV for C—O, 287.9 eV for C═O, 288.7 eV for O—C═O, and 284.4 eV for C—C bond, indicating that GO was enriched with oxygen functional groups. After reduction and magnetization, the C—C bond became the dominant peak as shown in the HRXPS C1s spectrum of SMG (Figure 3b). A small C−O tail at the higher binding energy region also appeared. This is also evident from the HRXPS O1s spectra of GO and SMG (Supporting Information Figure S2b), with one sharp peak at 533.3 eV in GO and a broad peak at ∼532.0 eV corresponding to the oxygen-containing functional groups in SMG. Figure 3c shows two dominant peaks at 711.24 and 724.6 eV corresponding to Fe $2p_{3/2}$ and Fe $2p_{1/2}$ of SMG, respectively. The spectral deconvolution indicates no satellite peaks around the binding energy 719.0 eV, which could be attributed to Fe_3O_4.[46] The results accorded well with the presence of an oxygen-containing peak in its O1s spectrum. The reduction of GO and the magnetization was further confirmed with XRD, Raman, TGA, and FTIR (Supporting Information Figures S3−S5).

Magnetic separation is an emerging technique capable of providing superior separation efficiency. The ease of manipulating magnetic NM by an external magnet greatly improves their recycling potential. The superparamagnetic property of SMG is apparent as shown in the magnetization curve at 298 K (Figure 4). The extrapolated saturation magnetization (M_s) of SMG is

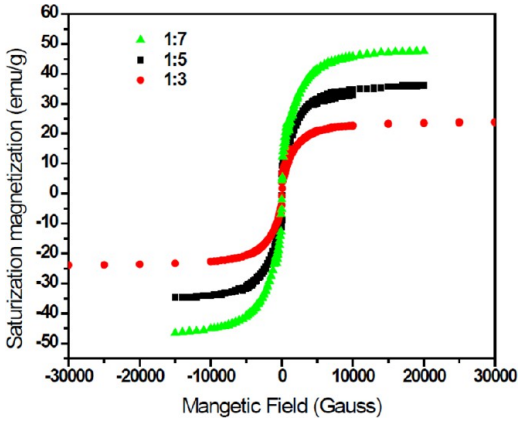

Figure 4. Saturation magnetization curves of SMG with different weight ratio of GO to ferrocene.

∼24.0 emu/g (1:3 GO to ferrocene weight ratio) which is ∼11.0% that of the bulk Fe (220 emu/g).[47] The M_s can be increased with higher ferrocene loading (up to 50 emu/g), indicating that SMG possesses superparamagnetic nature at room temperature. The obtained values of M_s were comparable to the literature reported values from other magnetic graphene and could be a preferred adsorbent for recycling experiments (Supporting Information Table S2). The measured BET surface area of SMG was ∼165 m^2/g (Supporting Information Figure S6) which is comparable to the literature reported value.[19]

Adsorption of Heavy Metals. We have carried out adsorption experiments at room temperature to study the effect of initial concentration and adsorption efficiency of different heavy metals. The effect of adsorption time, pH, and recycling abilities of SMG were investigated on Cr(VI). Aqueous solutions containing different heavy metal concentrations varying from 0.1 to 5.0 ppm, pH ∼6.5, and 2 h adsorption time were used for the experiment. The adsorption capacity of heavy metals was increased with increased initial concentration. The results were in good agreement with the *Langmuir adsorption isotherm* model (Figure 5a), which is expressed as follows: $q_e = abC_e/(1 + bC_e)$, where q_e (mg/g) is the equilibrium amount of heavy metal adsorbed per unit gram of the adsorbent, C_e (mg/L) is the equilibrium concentration of heavy metal, a (mg/g) is the maximum adsorption capacity, and b (L/mg) is a constant related to the free energy of adsorbent. The maximum adsorption capacity is 4.86, 3.26, and 6.00 mg/g for the removal of aqueous Cr(VI), As(V), and Pb(II) at an initial concentration of 5.0 ppm, respectively (Supporting Information Table S3). The maximum Cr(VI) adsorption capacity of SMG is higher than conventional adsorbents such as spheroidal cellulose (1.34 mg/g),[48] sugar cane bagasse (0.125 mg/g),[49] and NM based adsorbents such as nano-Fe_3O_4 based magnetic polymer (3.99 mg/g),[50] flower like α-Fe_3O_4 NPs (2.1 mg/g),[51] and mixed magnetite-maghemite NPs (0.6 mg/g),[52] (Supporting Information Table S4). Figure 5b shows the time profile of Cr(VI) adsorption by SMG at 1.0 ppm initial concentration operated in batch mode. The q_e value increased with increased adsorption time and leveled off after 100 min. The pH effect on Cr(VI) adsorption by SMG was shown in Figure 5c. The adsorption capacity is usually higher at lower pH, which is due to the positively charged nature of SMG promoting the electrostatic interactions[19] and the reduction of Cr(VI) to Cr(III) by unprotected ferrous ions and phenol functional groups on the surface of SMG.[53,54] Conversely, a decreasing trend was observed at higher pH, which is due to the increased net negative charges on the SMG surface. The HRXPS Cr2p spectrum of SMG-Cr (Figure 3d) shows that the $Cr2p_{3/2}$ and $Cr2p_{1/2}$ peaks are located at respective binding energy of 577.3 and 586.9 eV. The broad $Cr2p_{3/2}$ peak could be deconvoluted into two peaks at binding energies of 577.3 and 580.1 eV, which are characteristic of Cr(III) and Cr(VI).[55,56] This adsorption phenomenon is further supported by the SEM image of Cr(VI)-adsorbed SMG (SMG-Cr(VI)) (Supporting Information Figure S7b), which possesses wrinkled GO sheets (Supporting Information Figure S7a) with a rough surface. The energy dispersive X-ray pattern (Supporting Information Figure S7c) shows the presence of C, O, Cr, and Fe in SMG-Cr(VI). Overall, the removal of Cr(VI) involves the adsorption of Cr(VI) onto the SMG surface followed by reduction to Cr(III). The removal of As(V) also occurred through a simple physisorption mechanism at neutral pH (Supporting Information Figure S8a and b).[19] In the case of Pb(II), the Lewis acid−base interactions might dominate since graphene has rich π-electron clouds and Pb(II) is known to be electron deficient (Supporting Information Figures S8c and d).[57] Apart from Pb(II), we have also tested the adsorption efficacy of other cationic heavy metals such as Ag(I) and Hg(II) at the 1 ppm level which shows removal capabilities of 5 and 4.8 mg/g (data not shown). The sorption isotherms obtained at different temperatures (293, 313, and 333 K) clearly reveal that the adsorption of Cr(VI) increases with the temperature (Supporting Information Figure S9).

To further study the effect of interfering ions on Cr(VI) removal, we spiked different concentrations of Na_2SO_4 and KNO_3 with Cr(VI) (1 ppm) at pH 6.5. The result (Figure 5d)

dx.doi.org/10.1021/sc300112z | ACS Sustainable Chem. Eng. 2013, 1, 462−472

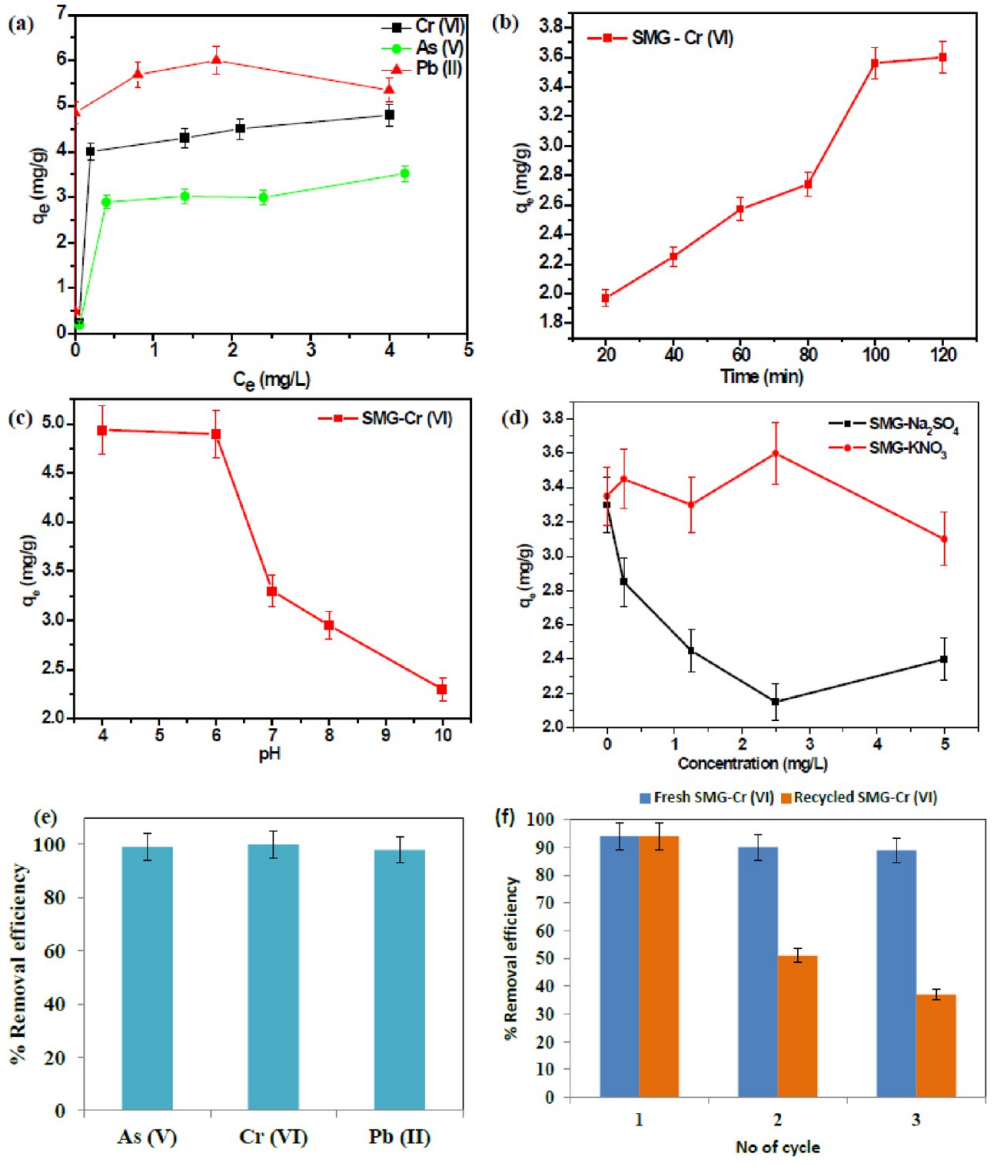

Figure 5. (a) Adsorption isotherm for Cr(VI), Pb(II), and As(V): the effect of (b) time, (c) pH, and (d) salt on Cr(VI) adsorption; (e) real water analysis; (f) acid/base washing cycle on Cr(VI) removal efficiency.

clearly shows that an increased Na_2SO_4 amount led to decreased trend of Cr(VI) adsorption, presumably due to (a) the SO_4^{2-} competing with Cr(VI) for adsorption sites and (b) surface complexation of SO_4^{2-} with Fe_2O_3 and thereby deactivation of the active sites available for Cr(VI). Conversely, KNO_3 did not exhibit any prominent effect on Cr(VI) adsorption, presumably due to the smaller negative charge on NO_3^- compared to SO_4^{2-}, which also holds true for NaCl.[58] A similar effect has been observed by Kundu et al.[59] The metal removal capability of SMG was further tested on DWS samples by premixing metal ions of different concentrations within the permissible limits of DWS levels. The adsorption experiments with SMG have achieved 99% removal capability (Figure 5e). Continuously adsorption experiments (Figure 5f) show the reusability potential of SMG for Cr(VI) adsorption by regenerating active sites on SMG by repeated washings with acid and base solutions. During the first adsorption, most of the surface adsorption sites were occupied by the heavy metals. As the adsoprtion was continued, the number of active sites available for the heavy metals subsequently decreased, and as a result, the adsorption capacity of SMG would be decreased.

Overall, the maximum heavy metal removal efficiencies by SMG were realized at initial concentrations ranging from 0.1−5.0 ppm, demonstrating that SMG is an effective adsorbent toward a wide range of heavy metals owing to its large specific surface area, high adsorption capacity, ease of magnetic separation, and recycling potential. However, SMG must be modified to possess a desired functionality for selective removal of specific heavy metal pollutants.

Disinfection control by SMG toward *Escherichia coli* (*E. coli*). The drinking water was often fouled with virus, fungi, and bacteria. The gram negative bacteria, *E. coli*, was often present in contaminated drinking water and monitored as a principle indicator.[60] *E. coli* was also detected in biofilm formed in water pipes made up of polyvinyl chloride, cast iron, and stainless steel.[61] We therefore studied the concentration-dependent disinfection control by SMG toward *E. coli* at different interaction times. Figure 6A represents the results of *E. coli* cell viability vs SMG concentration obtained by colony

dx.doi.org/10.1021/sc300112z | ACS Sustainable Chem. Eng. 2013, 1, 462−472

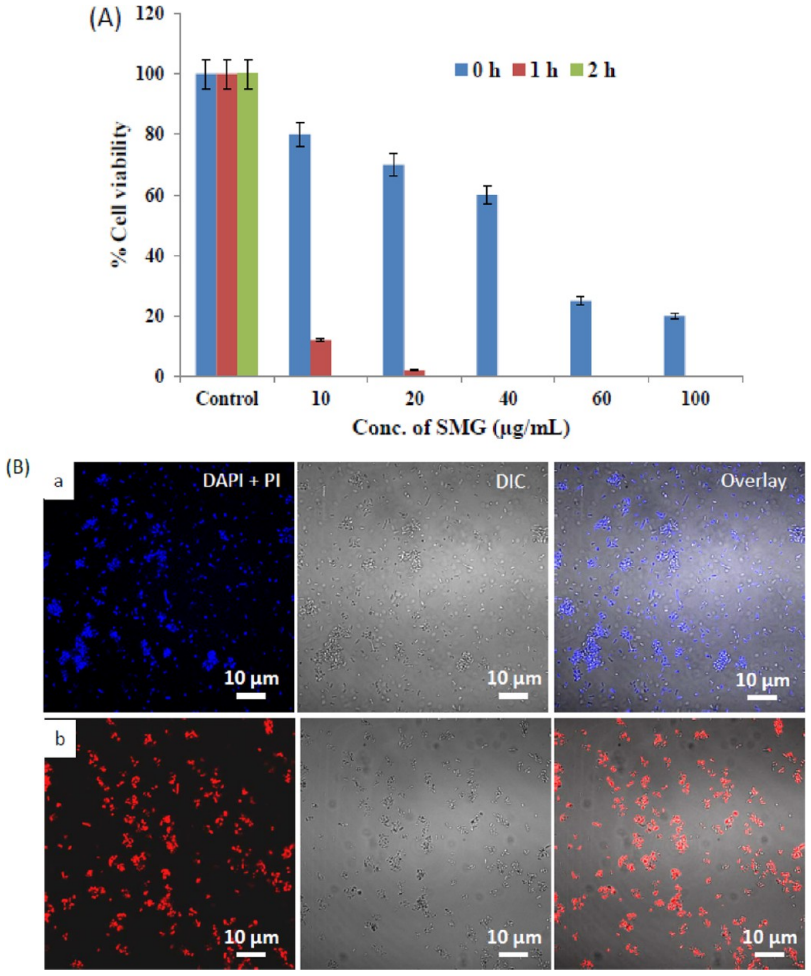

Figure 6. Interaction time and SMG concentration dependent disinfection control by SMG toward *E. coli*. (A) Cell viability obtained by plate count method and (B) confocal microscopy images for (a) control and (b) experimental (10 μg/mL SMG) stained with DAPI (blue color) and PI (red color).

count method at every hour (Supporting Information Figure S10).

The histogram shows decreased trend of cell viability with increased SMG concentration and interaction time. Interestingly, we observed that at higher SMG concentration (100 μg/mL) the killing action has started in few minutes and achieved 80% cell death. Extending the interaction time to 1 h, low SMG concentration (10 μg/mL) could achieve ∼90% killing efficacy and ∼95% was observed at higher SMG concentration (20 μg/mL). Figure 6B represents the confocal microscopy images of *E. coli* stained with DAPI (4′,6-diamidino-2-phenylindole) and PI (propidium iodide), which were known to identify the live and dead cells, respectively. Figure 6Ba represents the image of control bacterial cells permeable only to DAPI (blue color) but not PI (red color), indicating that most of the cells are alive. In contrast, Figure 6Bb show only PI positive cells, indicating that most cells were dead after interaction with low SMG concentration (10 μg/mL, Supporting Information Figure S11). The expected killing action is mostly due to the physical and/or mechanical disruption of the bacterial cell membrane due to the surface roughness of SMG (Supporting Information Figure S12), and thereby causing the release of cellular components.[62] There also exists another possibility that NMs cause oxidative stress and electron transfer mechanism between the graphene and bacterial cell wall, which is common among other graphene-based materials.[63] The disinfection control by SMG is better than other graphene-based NMs against *E. coli* in terms of shorter interaction time and lower concentration (Supporting Information Table S5). The reasons for rapid and effective killing of bacteria are presumably due to the following reasons: (a) dimensionality of the material—The CNT is one-dimensional, and graphene is two-dimensional in nature. The piercing action toward the bacterial cell membrane might be more predominant for graphene, owing to the possibility that four edges and corners of graphene basal plane could initiate this action; (b) surface roughness of SMG; (c) presence of hydrogen bonding interactions between −OH groups and bacterial cell membrane; and (d) bactericidal activity of Fe_3O_4 NPs present on the surface of SMG. All these factors might converge to the increased antibacterial activity of SMG.

However, there are still many disparities in the literature on graphene toxicity toward bacteria. For example, Akhavan et al. reported that graphene nanowalls have shown effective killing on *E. coli* and *S.aureus* than GO nanowalls.[64] Liu and Hu have reported that GO exhibits large extent of *E. coli* inhibition than that of graphene/reduced graphene oxide.[21,63] Ruiz et al. reported that GO can nonspecifically enhance the growth of *E. coli*.[65] In supporting to this, we also found that GO can enhance the bacterial growth in our experiments (the results are not provided here). The exploration on GO and graphene

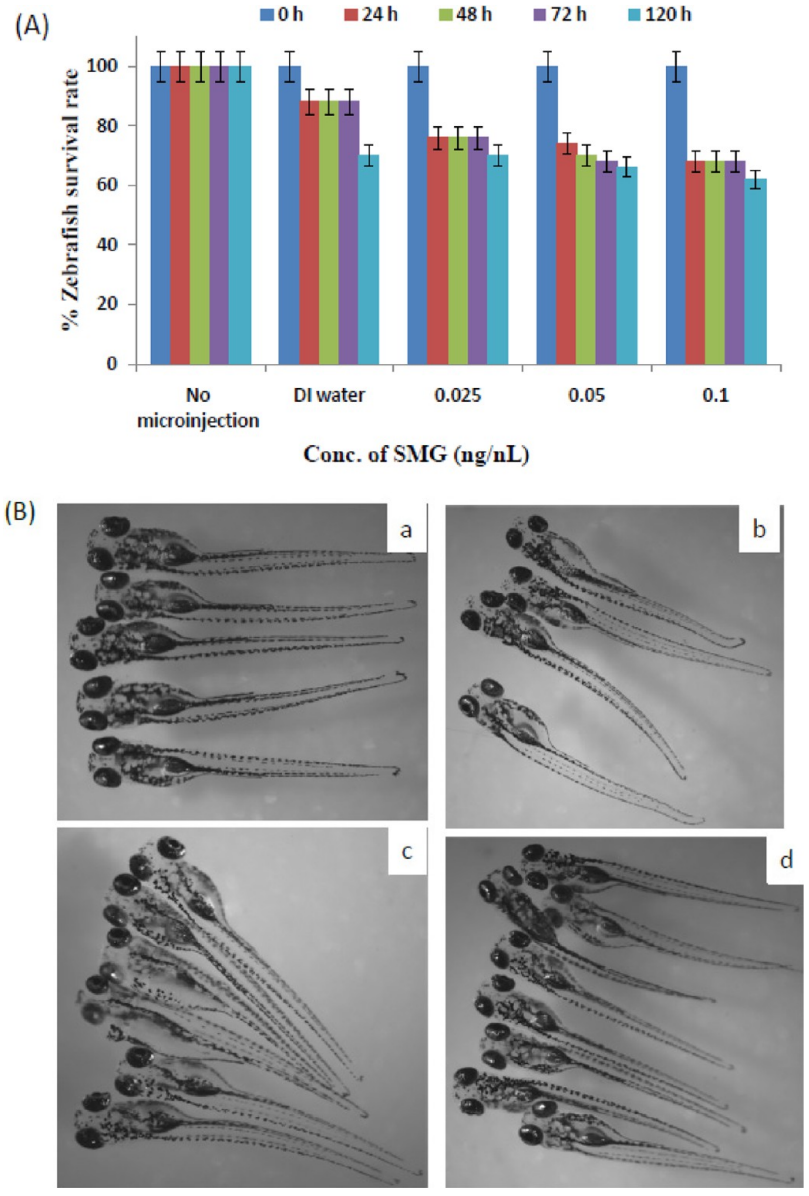

Figure 7. In vivo toxicity of SMG in zebrafish. (A) Survival rate up to 120 hpf. (B) DIC microscopy images after 120 hp for (a) control, (b) 0.025, (c) 0.05, and (d) 0.1 ng/nL SMG.

antibacterial activity and further detailed study is warranted. The effective antibacterial activity exhibied by SMG demonstrates it as a preferred disinfectant and good adsorbent for water purification and antimicrobial coatings.[66] Furthermore, the increased near-infrared (NIR) absorbance of SMG compared to GO[67] (Supporting Information Figure S13) provides an alternative disinfecting strategy such as photothermal therapy treating antibiotic-resistant pathogens, which became invulnerable by conventional antibiotics.[68,69]

In vivo Toxicity of SMG in Zebrafish. The presence of NMs in the environment is inevitable since our daily living is closely associated with their usage, implicating that addressing potential hazardous outcome is highly important.[5,70] Zebrafish are habitants living in river water. Their fast and transparent embryonic development as well as genomic similarity with humans made them as good animal model system for investigating the adverse effects by NMs-based adsorbents.[71] Figure 7A shows the concentration effect of SMG on zebrafish survival rate at the two cell stage (Supporting Information Figure S14) for every 24 h from 0 to 120 hpf (hours post fertilization). A decreased zebrafish survival rate at 120 hpf was apparent.

However, the extent of decrease was comparable to DI water injected embryos, elucidating that SMG did not exhibit any prominent toxicity toward zebrafish. The differential interference contrast (DIC) images in Figure 7B recorded after 120 hpf display the phenotypic changes in zebrafish after microinjection of SMG. Interestingly, there were no malformations observed in zebrafish subjected to SMG microinjection (Figure 7Bb–d). The morphology is quiet similar to that of normally developed zebrafish (Figure 7Ba). These results were in good agreement with our previous zebrafish toxicity study using multifunctional graphene.[72] Overall, the toxicity and deformations induced by carbon materials were less than other NMs such as Ag NPs and Cd^{2+} ions.[73,74]

dx.doi.org/10.1021/sc300112z | ACS Sustainable Chem. Eng. 2013, 1, 462–472

CONCLUSIONS

We have developed a rapid, green, and solvent-free microwave-assisted solid-state reaction for simultaneous reduction and magnetization of GO to yield SMG within 1 min. Salient features of SMG include increased adsorption sites and tunable superparamagnetic properties, facilitating the adsorption and magnetic separation of heavy metals from aqueous solutions such as Cr(VI), As(V), and Pb(II) down to the parts per billion levels over a wide range of pH and initial concentrations. Moreover, SMG exhibits disinfection action toward *E. coli* and desirable low toxicity toward zebrafish, making it a preferential adsorbent for safe drinking water. The discovery of SMG with greater adsorption capabilities and effective disinfection control with low toxicity and recyclability holds potential as a smart and cost-effective adsorbent for drinking water purification in future decentralized water systems.

ASSOCIATED CONTENT

Supporting Information

XRD, Raman, TGA, FTIR, bacterial plates, UV−vis-NIR, BET, zebrafish developmental stages, and SEM. This material is available free of charge via the Internet at http://pubs.acs.org.

AUTHOR INFORMATION

Corresponding Author

*Fax: +886 3 572 7774. Tel.: +886 3 572 1484. E-mail address: ycling@mx.nthu.edu.tw.

Notes

The authors declare no competing financial interest.

ACKNOWLEDGMENTS

We gratefully acknowledge the financial support by the National Science Council of Taiwan (NSC 101-2627-M-007-0051 and NSC101-2113-M-007-006-MY3) and National Tsing Hua University.

REFERENCES

(1) Omenn, G. S. Grand challenges and great opportunities in science, technology, and public policy. *Science* **2006**, *314*, 1696−1704.
(2) Lee, H. H.; Collins, J. J. Microbial environments confound antibiotic efficacy. *Nat. Chem. Biol.* **2012**, *8*, 6−9.
(3) McCall, M. J. Environmental, health and safety issues: Nanoparticles in the real world. *Nat. Nano.* **2011**, *6*, 613−614.
(4) Niu, H.; Wang, Y.; Zhang, X.; Meng, Z.; Cai, Y. Easy synthesis of surface-tunable carbon-encapsulated magnetic nanoparticles: adsorbents for selective isolation and preconcentration of organic pollutants. *ACS Appl. Mater. Interfaces* **2011**, *4*, 286−295.
(5) Teow, Y.; Asharani, P. V.; Hande, M. P.; Valiyaveettil, S. Health impact and safety of engineered nanomaterials. *Chem. Commun.* **2011**, *47*, 7025−7038.
(6) Shannon, M. A.; Bohn, P. W.; Elimelech, M.; Georgiadis, J. G.; Marinas, B. J.; Mayes, A. M. Science and technology for water purification in the coming decades. *Nature* **2008**, *452*, 301−310.
(7) Qin, F.; Zhao, Y.-Y.; Zhao, Y.; Boyd, J. M.; Zhou, W.; Li, X.-F. A toxic disinfection by-product, 2,6-Dichloro-1,4-benzoquinone, identified in drinking water. *Angew. Chem., Int. Ed.* **2010**, *49*, 790−792.
(8) Peter-Varbanets, M.; Zurbrügg, C.; Swartz, C.; Pronk, W. Decentralized systems for potable water and the potential of membrane technology. *Water Res.* **2009**, *43*, 245−265.
(9) Zhao, G.; Jiang, L.; He, Y.; Li, J.; Dong, H.; Wang, X.; Hu, W. Sulfonated graphene for persistent aromatic pollutant management. *Adv. Mater.* **2011**, *23*, 3959−3963.
(10) Zhang, D.; Wei, S.; Kaila, C.; Su, X.; Wu, J.; Karki, A. B.; Young, D. P.; Guo, Z. Carbon-stabilized iron nanoparticles for environmental remediation. *Nanoscale* **2010**, *2*, 917−919.
(11) Aposhian, H. V.; Aposhian, M. M. Arsenic Toxicology: Five Questions. *Chem. Res. Toxicol.* **2005**, *19*, 1−15.
(12) Huang, Z.-H.; Zheng, X.; Lv, W.; Wang, M.; Yang, Q.-H.; Kang, F. Adsorption of lead(II) ions from aqueous solution on low-temperature exfoliated graphene nanosheets. *Langmuir* **2011**, *27*, 7558−7562.
(13) Bailey, S. E.; Olin, T. J.; Bricka, R. M.; Adrian, D. D. A review of potentially low-cost sorbents for heavy metals. *Water Res.* **1999**, *33*, 2469−2479.
(14) Jiang, X.; Tay, J. H. Microbial community structures in a horizontal biotrickling filter degrading H2S and NH3. *Biores. Technol.* **2010**, *101*, 1635−1641.
(15) Pillay, K.; Cukrowska, E. M.; Coville, N. J. Multi-walled carbon nanotubes as adsorbents for the removal of parts per billion levels of hexavalent chromium from aqueous solution. *J. Hazard. Mater.* **2009**, *166*, 1067−1075.
(16) Liu, J.-F.; Zhao, Z.-s.; Jiang, G.-b. Coating Fe_3O_4 magnetic nanoparticles with humic acid for high efficient removal of heavy metals in water. *Environ. Sci. Technol.* **2008**, *42*, 6949−6954.
(17) Feng, Z.; Zhu, S.; Martins de Godoi, D. R.; Samia, A. C. S.; Scherson, D. Adsorption of Cd^{2+} on carboxyl-terminated superparamagnetic iron oxide nanoparticles. *Anal. Chem.* **2012**, *84*, 3764−3770.
(18) Sohn, K.; Kang, S. W.; Ahn, S.; Woo, M.; Yang, S.-K. Fe(0) Nanoparticles for nitrate reduction: stability, reactivity, and transformation. *Environ. Sci. Technol.* **2006**, *40*, 5514−5519.
(19) Chandra, V.; Park, J.; Chun, Y.; Lee, J. W.; Hwang, I.-C.; Kim, K. S. Water-dispersible magnetite-reduced graphene oxide composites for arsenic removal. *ACS Nano* **2010**, *4*, 3979−3986.
(20) Lin, Y.-T.; Huang, C.-P. Reduction of chromium(VI) by pyrite in dilute aqueous solutions. *Sep. Purif. Technol.* **2008**, *63*, 191−199.
(21) Hu, W.; Peng, C.; Luo, W.; Lv, M.; Li, X.; Li, D.; Huang, Q.; Fan, C. Graphene-Based Antibacterial Paper. *ACS Nano* **2010**, *4*, 4317−4323.
(22) Zhang, Y.; Ali, S. F.; Dervishi, E.; Xu, Y.; Li, Z.; Casciano, D.; Biris, A. S. Cytotoxicity effects of graphene and single-wall carbon nanotubes in neural phaeochromocytoma-derived PC12 cells. *ACS Nano* **2010**, *4*, 3181−3186.
(23) Allen, M. J.; Tung, V. C.; Kaner, R. B. Honeycomb carbon: a review of graphene. *Chem. Rev.* **2009**, *110*, 132−145.
(24) Liu, Q.; Shi, J.; Sun, J.; Wang, T.; Zeng, L.; Jiang, G. Graphene and graphene oxide sheets supported on silica as versatile and high-performance adsorbents for solid-phase extraction. *Angew. Chem., Int. Ed.* **2011**, *50*, 5913−5917.
(25) Gao, W.; Majumder, M.; Alemany, L. B.; Narayanan, T. N.; Ibarra, M. A.; Pradhan, B. K.; Ajayan, P. M. Engineered graphite oxide materials for application in water purification. *ACS Appl. Mater. Interfaces* **2011**, *3*, 1821−1826.
(26) Novoselov, K. S.; Geim, A. K.; Morozov, S. V.; Jiang, D.; Zhang, Y.; Dubonos, S. V.; Grigorieva, I. V.; Firsov, A. A. Electric field effect in atomically thin carbon films. *Science* **2004**, *306*, 666−669.
(27) Stankovich, S.; Dikin, D. A.; Piner, R. D.; Kohlhaas, K. A.; Kleinhammes, A.; Jia, Y.; Wu, Y.; Nguyen, S. T.; Ruoff, R. S. Synthesis of graphene-based nanosheets via chemical reduction of exfoliated graphite oxide. *Carbon* **2007**, *45*, 1558−1565.
(28) Gao, W.; Alemany, L. B.; Ci, L. J.; Ajayan, P. M. New insights into the structure and reduction of graphite oxide. *Nat. Chem.* **2009**, *1*, 403−408.
(29) Zhu, Y.; Murali, S.; Stoller, M. D.; Velamakanni, A.; Piner, R. D.; Ruoff, R. S. Microwave assisted exfoliation and reduction of graphite oxide for ultracapacitors. *Carbon* **2010**, *48*, 2118−2122.
(30) Skirtenko, N.; Tzanov, T.; Gedanken, A.; Rahimipour, S. One-step preparation of multifunctional chitosan microspheres by a simple sonochemical method. *Chem.—Eur. J.* **2010**, *16*, 562−567.

(31) Lee, P. L.; Chiu, Y. K.; Sun, Y. C.; Ling, Y. C. Synthesis of a hybrid material consisting of magnetic iron-oxide nanoparticles and carbon nanotubes as a gas adsorbent. *Carbon* **2010**, *48*, 1397−1404.
(32) Lee, P. L.; Sun, Y. C.; Ling, Y. C. Magnetic nano-adsorbent integrated with lab-on-valve system for trace analysis of multiple heavy metals. *Anal. At. Spectrometry* **2009**, *24*, 320−327.
(33) Gao, J.; Gu, H.; Xu, B. Multifunctional magnetic nanoparticles: design, synthesis, and biomedical applications. *Acc. Chem. Res.* **2009**, *42*, 1097−1107.
(34) Zhang, K.; Dwivedi, V.; Chi, C. Y.; Wu, J. S. Graphene oxide/ferric hydroxide composites for efficient arsenate removal from drinking water. *J. Hazard. Mater.* **2010**, *182*, 162−168.
(35) Koo, H. Y.; Lee, H.-J.; Go, H.-A.; Lee, Y. B.; Bae, T. S.; Kim, J. K.; Choi, W. S. Graphene-based multifunctional iron oxide nanosheets with tunable properties. *Chem.—Eur. J.* **2011**, *17*, 1214−1219.
(36) Jabeen, H.; Chandra, V.; Jung, S.; Lee, J. W.; Kim, K. S.; Kim, S. B. Enhanced Cr(VI) removal using iron nanoparticle decorated graphene. *Nanoscale* **2011**, *3*, 3583−3585.
(37) Zhu, J.; Wei, S.; Gu, H.; Rapole, S. B.; Wang, Q.; Luo, Z.; Haldolaarachchige, N.; Young, D. P.; Guo, Z. One-pot synthesis of magnetic graphene nanocomposites decorated with core@double-shell nanoparticles for fast chromium removal. *Environ. Sci. Technol.* **2011**, *46*, 977−985.
(38) Liu, M.; Chen, C.; Hu, J.; Wu, X.; Wang, X. Synthesis of magnetite/graphene oxide composite and application for cobalt(II) removal. *J. Phys. Chem. C* **2011**, *115*, 25234−25240.
(39) Li, J.; Zhang, S.; Chen, C.; Zhao, G.; Yang, X.; Li, J.; Wang, X. Removal of Cu(II) and fulvic acid by graphene oxide nanosheets decorated with Fe_3O_4 nanoparticles. *ACS Appl. Mater. Interfaces* **2012**, *4*, 4991−5000.
(40) Sreeprasad, T. S.; Maliyekkal, S. M.; Lisha, K. P.; Pradeep, T. Reduced graphene oxide-metal/metal oxide composites: facile synthesis and application in water purification. *J. Hazard. Mater.* **2011**, *186*, 921−931.
(41) Sen Gupta, S.; Sreeprasad, T. S.; Maliyekkal, S. M.; Das, S. K.; Pradeep, T. Graphene from sugar and its application in water purification. *ACS Appl. Mater. Interfaces* **2012**, *4*, 4156−4163.
(42) Bai, S.; Shen, X.; Zhong, X.; Liu, Y.; Zhu, G.; Xu, X.; Chen, K. One-pot solvothermal preparation of magnetic reduced graphene oxide-ferrite hybrids for organic dye removal. *Carbon* **2012**, *50*, 2337−2346.
(43) Hummers, W. S.; Offeman, R. E. Preparation of graphitic oxide. *J. Am. Chem. Soc.* **1958**, *80*, 1339−1339.
(44) Liang, Y.-C.; Hwang, K. C.; Lo, S.-C. Solid-state microwave-arcing-induced formation and surface functionalization of core/shell metal/carbon nanoparticles. *Small* **2008**, *4*, 405−409.
(45) Louchev, O. A.; Hester, J. R. Kinetic pathways of carbon nanotube nucleation from graphitic nanofragments. *J. Appl. Phys.* **2003**, *94*, 2002−2010.
(46) Mills, P. S., J. L. A study of the core level electrons in iron and its three oxides by means of x-ray photoelectron spectroscopy. *J. Phys. D Appl. Phys.* **1983**, *16*, 723−732.
(47) Felner, I.; Nowik, I.; Prilutskiy, E. *Mössbauer and magnetic studies of nanosize* $(Fe,Co)_x$ C_{1-X} *alloys*; Springer: Berlin Heidelberg, 2009; pp 189−195.
(48) Liu, M. Z.; Hong; Zhang, X.; Deng, Y.; Liu, W.; Zhan, H. Removal and recovery of chromium(III) from aqueous solutions by a spheroidal cellulose adsorbent. *Wat. Envron. Res.* **2001**, *73*, 322−328.
(49) Sharma, D. C.; Forster, C. F. A preliminary examination into the adsorption of hexavalent chromium using low-cost adsorbents. *Biores. Technol.* **1994**, *47*, 257−264.
(50) Zhao, Y.-G.; Shen, H.-Y.; Pan, S.-D.; Hu, M.-Q.; Xia, Q.-H. Preparation and characterization of amino-functionalized nano-Fe_3O_4 magnetic polymer adsorbents for removal of chromium(VI) ions. *J. Mater. Sci.* **2010**, *45*, 5291−5301.
(51) Zhong, L. S.; Hu, J. S.; Liang, H. P.; Cao, A. M.; Song, W. G.; Wan, L. J. Self-assembled 3D flowerlike iron oxide nanostructures and their application in water treatment. *Adv. Mater.* **2006**, *18*, 2426−2431.
(52) Chowdhury, S. R.; Yanful, E. K. Arsenic and chromium removal by mixed magnetite-maghemite nanoparticles and the effect of phosphate on removal. *J. Environ. Manage.* **2010**, *91*, 2238−2247.
(53) Cao, J.; Zhang, W.-X. Stabilization of chromium ore processing residue (COPR) with nanoscale iron particles. *J. Hazard. Mater.* **2006**, *132*, 213−219.
(54) Hsu, N.-H.; Wang, S.-L.; Lin, Y.-C.; Sheng, G. D.; Lee, J.-F. Reduction of Cr(VI) by crop-residue-derived black carbon. *Environ. Sci. Technol.* **2009**, *43*, 8801−8806.
(55) Ai, Z.; Cheng, Y.; Zhang, L.; Qiu, J. Efficient removal of Cr (VI) from aqueous solution with $Fe@Fe_2O_3$ core−shell nanowires. *Environ. Sci. Technol.* **2008**, *42*, 6955−6960.
(56) Liang-wen, X.; Shihong, L.; Bi-xian, P. Mechanism of hologram formation in dichromated gelatin with x-ray photoelectron spectroscopy. *Appl. Opt.* **1998**, *37*, 3678−3684.
(57) Machida, M.; Mochimaru, T.; Tatsumoto, H. Lead(II) adsorption onto the graphene layer of carbonaceous materials in aqueous solution. *Carbon* **2006**, *44*, 2681−2688.
(58) Wang, X. S.; Chen, L. F.; Li, F. Y.; Chen, K. L.; Wan, W. Y.; Tang, Y. J. Removal of Cr (VI) with wheat-residue derived black carbon: reaction mechanism and adsorption performance. *J. Hazard. Mater.* **2010**, *175*, 816−822.
(59) Bhakat, P. B.; Gupta, A. K.; Ayoob, S.; Kundu, S. Investigations on arsenic(V) removal by modified calcined bauxite. *Colloids Surf., A* **2006**, *281*, 237−245.
(60) Jacobs, H. The hitchhiker's guide to E. coli. *EMBO Rep.* **2011**, *12*, 1205−1205.
(61) Juhna, T.; Birzniece, D.; Larsson, S.; Zulenkovs, D.; Sharipo, A.; Azevedo, N. F.; Ménard-Szczebara, F.; Castagnet, S.; Féliers, C.; Keevil, C. W. Detection of escherichia coli in biofilms from pipe samples and coupons in drinking water distribution networks. *Appl. Environ. Microbiol.* **2007**, *73*, 7456−7464.
(62) Liu, S.; Wei, L.; Hao, L.; Fang, N.; Chang, M. W.; Xu, R.; Yang, Y.; Chen, Y. Sharper and faster "nano darts" kill more bacteria: a study of antibacterial activity of individually dispersed pristine single-walled carbon nanotube. *ACS Nano* **2009**, *3*, 3891−3902.
(63) Liu, S.; Zeng, T. H.; Hofmann, M.; Burcombe, E.; Wei, J.; Jiang, R.; Kong, J.; Chen, Y. Antibacterial activity of graphite, graphite oxide, graphene oxide, and reduced graphene oxide: membrane and oxidative stress. *ACS Nano* **2011**, *5*, 6971−6980.
(64) Akhavan, O.; Ghaderi, E. Toxicity of graphene and graphene oxide nanowalls against bacteria. *ACS Nano* **2010**, *4*, 5731−5736.
(65) Ruiz, O. N.; Fernando, K. A. S.; Wang, B.; Brown, N. A.; Luo, P. G.; McNamara, N. D.; Vangsness, M.; Sun, Y.-P.; Bunker, C. E. Graphene oxide: a nonspecific enhancer of cellular growth. *ACS Nano* **2011**, *5*, 8100−8107.
(66) Ghule, K.; Ghule, A. V.; Chen, B.-J.; Ling, Y.-C. Preparation and characterization of ZnO nanoparticles coated paper and its antibacterial activity study. *Green Chem.* **2006**, *8*, 1034−1041.
(67) Robinson, J. T.; Tabakman, S. M.; Liang, Y.; Wang, H.; Sanchez Casalongue, H.; Vinh, D.; Dai, H. Ultrasmall reduced graphene oxide with high near-infrared absorbance for photothermal therapy. *J. Am. Chem. Soc.* **2011**, *133*, 6825−6831.
(68) Norman, R. S.; Stone, J. W.; Gole, A.; Murphy, C. J.; Sabo-Attwood, T. L. Targeted photothermal lysis of the pathogenic bacteria, pseudomonas aeruginosa, with gold nanorods. *Nano Lett.* **2007**, *8*, 302−306.
(69) Wu, M.-C.; Deokar, A. R.; Liao, J.-H.; Shih, P.-Y.; Ling, Y.-C. Graphene-based photothermal agent for rapid and effective killing of bacteria. *ACS Nano* **2013**, 1281−1290.
(70) Duncan, T. V. The communication challenges presented by nanofoods. *Nat. Nano* **2011**, *6*, 683−688.
(71) Spence, R.; F., M. K.; Reichard, M.; Hua, K. A.; Wahab, M. A.; Ahmed, Z. F.; Sith, C. The distribution and habitat preferences of the zebrafish in Bangladesh. *J. Fish Biol.* **2006**, *69*, 1435−1448.
(72) Gollavelli, G.; Ling, Y.-C. Multi-functional graphene as an in vitro and in vivo imaging probe. *Biomaterials* **2012**, *33*, 2532−2545.
(73) Lee, K. J.; Nallathamby, P. D.; Browning, L. M.; Osgood, C. J.; Xu, X.-H. N. In vivo imaging of transport and biocompatibility of

single silver nanoparticles in early development of zebrafish embryos. *ACS Nano* **2007**, *1*, 133−143.
(74) Hallare, A. V.; Schirling, M.; Luckenbach, T.; Köhler, H. R.; Triebskorn, R. Combined effects of temperature and cadmium on developmental parameters and biomarker responses in zebrafish (Danio rerio) embryos. *J. Ther. Biol.* **2005**, *30*, 7−17.